Monitoring of seasonal variability and movement of suspended sediment concentration along Thiruvananthapuram coast, South India using Landsat OLI sensor

Bismay Ranjan Tripathy[1], Kaliraj Seenipandi[1], Haroon Sajjad[2], Pawan Kumar Joshi[3], Bhagwan Singh Chaudhary[4] and PavanKumar[2,*]

[1]National Centre for Earth Science Studies, Ministry of Earth Sciences, Govt. of India, Thiruvananthapuram - 695011, India
[2]Department of Geography Jamia Millia Islamia, New Delhi, India
[3]School of Environmental Science, Jawaharlal Nehru University, New Delhi, India
[4]Department of Geophysics, Kurukshetra University, Kurukshetra, Haryana, India

Correspondence to: Pavan Kumar (pavan.jamia@gmail.com)

Abstract.

Studies on suspended sediment concentration at seasonal scale play a vital role for understanding coastal hydrodynamic processes in an area. Assessment of spatio-temporal changes in suspended sediments along the near offshore has more complexity using conventional method; this issues nowadays can successfully be solved using multi-temporal remotely sensed images with the help of advanced image processing techniques. The present study is an attempt to demonstrate the model algorithm used to extract suspended sediment concentration using Landsat 8 OLI (Operational Land Imager) sensor image. The study has been executed along the near-offshore area of Thiruvananthapuram coast, South India for extraction of suspended sediment and its seasonal variability during pre and post monsoon. The OLI images were pre-processed for obtaining the actual reflectance using FLASSH module of ENVI v5.5 software. The generic model developed here in is designed to compute the spectral reflectance variability between coastal water and suspended sediments and to differentiate the spatial accumulation of suspended sediments concentration from the coastal water at pixel scale. Maximum (0.8 % in near infrared) and minimum (0.6% in blue) spectral reflectance indicates the occurrence of suspended sediments in the coastal water. The model-derived results revealed that the suspended sediment gradually decreased with the increase of depth and distance from the shoreline. Higher sediment concentration was accumulated along lower depth in coastal water due to action of wave and current that circulated sediments seasonally. The higher concentration of suspended sediment load was

estimated as 0.92 mg/l within the shallow depth (< 10m) of the coastal water and 0.30 mg/l at the depth of 30 m. Seasonal variability of suspended sediments was observed towards north - south direction during the pre-monsoon; where it significantly moves reversely during post-monsoon. The spatial variability of suspended sediments was indirectly proportional to depth and distance from the shoreline; and directly proportional to wave and littoral current along the offshore. The study proves that the developed model with computational algorithm can be used as an effective tool for estimation of suspended sediment using multi-temporal OLI image; the output may be helpful for coastal zone management and conservation planning and development.

1 Introduction

Suspended loads are generally the portion of sediments, which contain fine sand, silt and clay etc and are carried to the ocean by the action of the fluid. These particles settle in such a way that they certainly do not touché the bed, which is maintained by means of turbulence of flowing water. Therefore, it is necessary to measure and monitor the suspended sediments in the ocean transported by various agents for flood hazard management, water resource planning, climate and ecology studies (Whitelock, *et al*., 1981; Sinha *et al*., 2004). Extracting information as suspended sediment concentration (SSC) in coastal waters is very important for assessment and monitoring of coastal settings and their effects on their ecology. A large number of noteworthy researches have been conducted on the spatiotemporal deviation in suspended sediments concentration (SSC) in a system all over the world (Kaliraj and Chandrasekar, 2012). However, monitoring and measurement of such suspended sediments is extremely difficult due to dynamic unit distance and factors acting on it. Consequently, since the last few decades, attention has been paid to the potential of satellite data to measure and monitor the movement of SSC in ocean (Nechad, *et al.* 2010; Ontowirjo, *et al*., 2013; Rawat *et al*., 2011; Curran *et al*., 1988). Remote sensing offers larger aerial view for analyzing water quality and provides a more efficient cost effective method for assessing SSC from the ocean. Geospatial technology has been widely used by many hydrologists, as it has the ability to answer complex, spatial and temporal questions. (Marcus and Fonstad, 2010; Panwar *et al*., 2017).

Presently satellite technology is opted over marine surveys to assess the distribution and movement of suspended sediments because the cost of application is lower than that of site marine survey as it replaces the requirement for a large number of monitoring positions with a single satellite (Byers, 1992). It performs as an influential tool for mapping suspended sediments in the ocean, which has been discharged by a various sources like; river, stream, industries and urban residues. Images taken by optical devices boarded on the satellites and field observation data help in regular monitoring of suspended sediment transportation (Gerald, 1980; Kaliraj and Chandrasekar, 2012). However, it is hindered by two vital difficulties. First, remotely sensed data can detect the suspended sediments in the upper few meters of the water layers. Thus it is necessity to convert it into a depth-integrated load before evaluation for numerical models and field measurements. Second, numerous approaches are dependent on the observed relationship between water-leaving reflectance and SSC analyzed through remote sensing tools. Experimental corrections provide site-specific calculations of water quality parameters with practical accuracy by using field derived reflectance data. Spectral examination of satellite imagery is based on the calculation of reflected electromagnetic solar radiation, which is used to evaluate turbidity and SSC. Depending on reflection and absorption of different wavelengths, unique signature and curves are produced (Islam, *et al*., 2001; Kaliraj, *et al*., 2013a; Kaliraj, *et al*., 2013b).

Remotely sensed data can only provide information in one-two dimensional forms because, it cannot give evidence on the vertical circulation of sediments in water as we get the reflection data from only two-meter surface water (Tassan, 1998). Two/three-dimensional information using remote sensing data is of less value as the data is not vertically averaged. Oceanic survey, on the other hand, can be modelled for three dimensions as it is the average data of vertically through the water column to horizontally across the surface of the water. Thus, a comprehensive series of sample acquisition throughout the water column is essential for assessing the vertical sediment distribution (Katlane, *et al*., 2013; Warrick*et al*., 2004). Wavelength between 0.5 and 0.8 micrometer is used for remote sensing for detecting suspended sediments, which includes the visible, green, red and near infra-red light. Colour and turbidity in the water, affect the energy level (visible, very near ultraviolet and infra-red wavelengths) which is sensed by a camera or scanner. Energy flux decreases with increase in colour (due to absorption of solar energy) and the flux increases with an increase in turbidity (due to reflection of solar energy). As

solar energy is reflected but that sensed data cannot be used directly as it contains atmospheric errors, which need to be corrected before its further use (Wang and Lu 2010; Qu, 2014; Yanjiao et al., 2007; Zhang et al., 2003).

Various scholars have used simple sediment rating curve and support vector regression statistical method to estimate SSC (Kisi 2012, Gao 2008). These methods were limited to a single river or water body and did not take into consideration the effect of particle size distribution and water temperature. Thus, more efficient methods are required to analyze SSC variability. The suspended sediments are generally derived from the discharge of river, shore erosion and weathering of rocky shore that can control the creation of coastal headlands and provide source material to the physical, chemical and biological inputs in the offshore (Whitelock et al., 1981, Kronvang et al., 1997).

The study attempts to monitor the suspended sediments, using Landsat 8 (OLI) at Thiruvananthapuram district coast; we first corrected atmospheric errors in the data and then converted it into marine reflectance. The specific objectives of the study were to monitor seasonal variation in suspended sediment concentration and to assess movement of suspended sediments during pre and post-monsoon. Suspended fine grain sediments are deposited offshore in deeper water where the bottom is stirred only. The lower part of coast was observed with heavy deposition during the pre-monsoon as the swashing of suspended particles by less energy waves along with the dominant wave direction in this session. Whereas, in the post monsoon the accumulation of the sediments found to be at middle part of the study area as due to the wave and current action at that particularly season.

2 Study area

The coastal zone of the Thiruvananthapuram District of Kerala in India covers a stretch of about 72 km extending seaward for 10 km from the coast bound. The geographical extent of the area is between 8°17' N and 8°54' N latitudes and 76°41' E and 77°17' E longitudes (Fig. 1). The coastal stretch is highly dynamic due to the hydrodynamic forces such as waves, currents and tides, etc. It has also undergone changes in near shore bathymetry and landforms. Natural and anthropogenic activities have caused morphological instability in the landform along the coast. Commercial activities, tourist's sites, dense

population and thick settlement are characteristic features of major locations of the coastal stretch. Along the coast, human settlements and properties are threatened due to severe coastal erosion. The study area enjoys a sub-tropical climate. It receives average annual rainfall varying between 826 mm and 1456 mm. It experiences mean annual temperature ranging between 23.78 ^{0}C and 33.95^{0} C (Meteorological Center, IMD, Thiruvananthapuram (https://www.imdtvm.gov.in).

<Insert Fig. 1 Location map of study area>

3 Material and methodology

3.1 Data used

We used OLI data for determining pre-monsoon (March 2017) and post-monsoon (September 2017) suspended sediments. Operation Land Imager gives the multispectral data for visible as well as infrared range. It covers the entire earth in 16 days. The OLI uses the push broom sensor with 115-mile cross-track field of view.

Digital Bathymetry Model (DBM) was utilized for extracting the bathymetry. Shuttle radar topography mission is a research effort that obtained digital elevation model for generating high-resolution digital topography database for the earth. For extracting the bathymetry, we have used a global relief model which composite model of Digital Bathymetry Model (DBM). SRTM30_PLUS (http://topex.ucsd.edu/WWW_html/srtm30_plus.html) consists of both topography and bathymetry model that provides 30 arc seconds (900 m) resolution data for land as well as for Ocean, which is derived from depth sounding (SONAR) and satellite altimetry. Finally, the wind direction is derived from the portal ERA (European Reanalysis) Interim, provided by ECMWF (European Centre for Medium-Range Weather Forecasts), which is an independent intergovernmental organisation, based on a four-dimensional IFS (Cy31r2) system.

3.2 Conversion of DN to TOA reflectance

Atmospheric correction was done to determine the water-leaving reflectance (ratio of upwelling radiance just above the water surface and the solar down welling irradiance) by eliminating the contribution of surface glint and atmospheric

scattering from the estimated total reflectance. The total atmospheric reflectance was estimated as the sum of the molecular reflectance (Rayleigh's reflectance), specular reflection of the sun and the reflectance of aerosol, foam and whitecaps. All these parameters were determined from the metadata and field measurement, using empirical relationship (Gordon and Wang, 1994). Solar radiation is totally absorbed by water in NIR band. Thus, water-leaving radiance can be eliminated to estimate aerosol directly. Hence, medium to relatively high suspended particulate matter (SPM) concentration can better be mapped by using near-infrared and red bands.

These raw data can be converted to ToA Reflectance from DN (eq. i), using rescaling factors and parameters found in the metadata file (MTL.txt) provided with the data.

$$\rho_t' = (M_p)(Q_{cal}) + (A_r) \quad \text{(i)}$$

Where;

ρ_t'= TOA planetary reflectance (without solar angle correction)

M_p= Band-specific multiplicative rescaling factor

A_r =Band-specific additive rescaling factor

Q_{cal}= Quantized and calibrated standard product pixel values (DN)

Next, we have corrected the ρ_t'using eq. ii for the solar angle;

$$\rho_t = \frac{\rho_t'}{\cos(\theta_{SZ})}$$

$$= \frac{\rho_t'}{\sin(\theta_{SE})} \quad \text{(ii)}$$

Where;

ρ_t = TOA planetary reflectance

θ_{SE}= Local sun elevation angle

θ_{SZ}= Local solar zenith angle

θ_{SZ}= 90° - θ_{SE}.

3.3 Molecular/ Rayleigh's reflectance correction

Most Reflectance from air molecules and aerosols must be accurately modeled and removed from the observed signal. At-sensor total reflectance (eq.iii) can be expressed as the following formula.

$$\rho_{TOA} = \frac{L_1B\_Radiance}{ExtraTerrestrialSunRadiation} \quad \text{(iii)}$$

After the Rayleigh correction, ground surface + aerosol albedo r_{as} can be determined as:

$$\rho_{0.5} = [\,\rho_{TOA} - \rho_R/T_R]/\,[1 + S_R\,(\rho_{TOA} - \rho_R/T_R)] \text{(iv)}$$

Where;

ρ_r= Rayleigh reflectance

Extra Terrestrial Sun Radiation = $(\pi)(E_S)(\cos(\theta_S))\,(d_{sol})\exp\,[(-m)(\tau_{net})]$

$$m = \frac{1}{\cos\,(\theta_s)} + \frac{1}{\cos\,(\theta_v)}$$

$\theta_s$andθ_v are the angle of solar zenith and sensor zenith respectively

$d_{sol}$is the eccentricity correction factor of the earth' s orbit

T_R = Rayleigh atmospheric transmittance

$$T_{total} = (T_{yu})(\,T_{yd})\,\exp\,[(-m)(\tau_{O_2})]\exp\,[(-m)(\tau_{watervapour})]$$

T_{yu} =Rayleigh transmittance for sensor

$$T_{yu} = \frac{2/3 + \cos(\theta_v) + (2/3 - \cos(\theta_v)) \exp\left[-\left(\tau_{Raylight}\right)/(\cos(\theta_v)\right]}{4/3 + \tau_{Raylight}}$$

167 T_{yd} = Rayleigh transmittance for sun

$$T_{yd} = \frac{2/3 + \cos(\theta_s) + (2/3 - \cos(\theta_s)) \exp\left[-\left(\tau_{Raylight}\right)/(\cos(\theta_s)\right]}{4/3 + \tau_{Raylight}}$$

168

Where;

169 $\tau_{Raylight}$ = Rayleigh optical depth

170 τ_{O_2} = Oxygen optical depth

171 τ = Optical depth

172 S_R= Rayleigh spherical albedo

173

$$RayPolynomi = -0.58 + \tau_{Raylight} - 0.25\left(\tau_{Raylight}\right)^2 + 0.055\left(\tau_{Raylight}\right)^3 - 0.0098\left(\tau_{Raylight}\right)^4 + 0.0011(\tau_{Raylight})^5$$

174

175 Rayleigh reflectance (ρ_r) is calculated below;

$$\rho_r = (\mu_s, \mu_v, \emptyset_v - \emptyset_s) = \rho_{R1}(\mu_s, \mu_v, \emptyset_v - \emptyset_s) + (1 - \exp[-(\tau)/(\mu_v)] * (1 - \exp[-(\tau)/(\mu_v)]\Delta(\tau) \quad \text{(v)}$$

176

177

178 Where;

179 μ_s=cos of sun zenith

180 μ_v= cos of sensor zenith

$\emptyset_v$= sun azimuth

$\emptyset_s$= sensor azimuth

ρ_{R1}= the single-scattering contribution

τ = Atmospheric optical depth

Sensor spectral response based pre-computed radaitive transfer simulations, solar and sensor viewing geometry and ancillary information were used to estimate most of the components of the above equations. Rayleigh correction was executed by subtracting the Rayleigh reflectance value from the top of atmosphere reflectance as:

$$\rho_c = \rho_R - \rho_{TOA} \text{(vi)}$$

3.4 Marine Reflectance Calculation

Aerosol reflectance (ε) over water pixel was derived from the ratio of reflectance in the couple of bands. "ε"; the proportion of multiple-scattering aerosol reflectance was constant over the part. The value of ε was considered as 1 for getting standard processing in VR and NIR bands (Vanhellemont *et al*., 2014). A linear relation was established between marine reflectance and constant aerosol type (ε). Aerosol can be determined through slope of the regression line (Neukermans, *et al*., 2009) and the median ratio of Rayleigh corrected reflectance in bands 4 and 5 (ρc^4, ρc^5). Alpha, "∝", the ratio of oceanic reflectance was determined by using the average resemblance spectrum for the band central wavelengths:

$$\propto = \frac{{\rho_w}^{(4)}}{{\rho_w}^{(5)}} = \frac{{\overline{\rho}_{wn780}}^{(655nm)}}{{\overline{\rho}_{wn780}}^{(865nm)}} = \frac{4.734}{0.544} = 8.702 \quad \text{(vii)}$$

Gamma, "γ" is the fraction of diffused atmospheric transmittances in the two bands, which is calculated using the following equation (eq. viii).

$$\gamma = ({t_0}^{(4)})({t_v}^{(4)})/({t_0}^{(5)})({t_v}^{(5)}) \quad \text{(viii)}$$

Then, the oceanic reflectance is calculated using $\rho_w{}^{(3)}$ and $\rho_w{}^{(4)}$ as noted eq. ix

$$\rho_w{}^{(3)} = \frac{\alpha}{t_0{}^{(4)} t_v{}^{(4)}} \left[\frac{\rho_c{}^{(3)} - \rho_c{}^{(4)}}{\alpha\gamma - \varepsilon} \right] \qquad \text{(ix)}$$

3.5 Spectral analysis of the suspended sediments

The reflectance spectrum of an object is a graph of the radiation reflected to the incident wavelength and serves as a unique signature for the particular object. The water curve is characterized by a high absorption at near-infrared wavelength and beyond, whereas maximum reflectance at blue. The spectral curve for SSC is plotted for suspended particles in the ocean at a certain wavelength, after getting marine reflectance and correcting the aerosol from the data.

3.6 Extraction of suspended sediments and its validation

After getting the error free reflectance data, we have proceeded for mapping the movement of suspended sediments during pre-monsoon and post-monsoon seasons. Increment in red reflectance in the turbid water indicates the presence of sediments. We determined suspended solid matter using the single band (Red band) algorithm (eq.x) used by Nechad *et al*., 2010.

$$SPM = (A)\left(\frac{\rho_w}{1}\right) - \frac{\rho_w}{c} - - - - - (x)$$

Where;

A = 327.84 g/m^3

C = 0.1708.

So in this way we have mapped the solid particles suspended near the shore (within 10 km) and get the idea about transportation of suspended particle along the coast during pre and post monsoon seasons.

Single band algorithm, which is suitable for the study area, was used as a predictor for assessing the suspended sediments along the coast. The model was validated with samples collected within 5 km along the coast. Root mean square error (RMSE) was calculated (eq. xi) for examining the variation between the field based predicted ($\hat{y}$) data and satellite based observed (y) data values. The study used the concurrent satellite as well as ground data for better calibration.

$$RMSE = \sqrt{\frac{\hat{y} - y}{n}} - - - - - - (xi)$$

4 Results

The sources of suspended sediments are generally from the discharge of river, shore erosion and weathering of rocky shore. These sources control the creation of coastal headlands and provide source material to the physical, chemical and biological inputs in the offshore. The coastal region accumulated with suspended sediments changes the coastal morphology. The sediments near the shore are transported instead of being stable at a place due to various hydrodynamic action influences of the ocean such as mean significant wave height (Fig. 2). Significant wave height can be calculated as the average height of the one-third of the measured waves (eq. xii), which are N in numbers, having the largest wave height:

$$H_{1/3} = \frac{1}{\frac{1}{3}N} \sum_{m=1}^{\frac{1}{3}N} H_m \; - - - - - (xii)$$

The individual wave heights (H_m) is classified with highest wave having m=1 and the lowest wave having m=N. One-third of the measured waves is used as it corresponds best with visual observations of experienced mariners. It is evident from the figure that the mean significant wave height is high for the southern part of the study area, which decreases towards the north. High wave energy can mingle more sediments in that region compared to less energy influential area, as it does not let the sediments transport to other places.

<Insert Fig. 2 Mean significant wave height along the coast>

4.1 Spectral signature of water and SSC having different magnitudes

The reflectance curve is plotted between the wavelength and the detected suspended sediments' reflectance from the large area of 900 sq. meters (30 meter resolution). The reflectance variation of the surface water indicates the presence of suspended sediments along the off-shore (Fig.3). We can perceive that the regions having high suspended sediments have high reflectance in the NIR wavelength and the regions having comparatively less suspended sediments have high reflectance in the red wavelength. The area having no suspended sediments shows high reflectance in the blue wavelength and total absorption in the NIR wavelength. Hence reflectance curve helped to determine the concentration of suspended sediments in the water.

<Insert Fig. 3 Spectral reflectance of SSC in different wavelength of OLI image>

4.2 Monitoring of Suspended Sediments

The northern part of study area experienced heavy deposition during the post-monsoon as the suspended particles swashed by fewer energy waves along with the dominant wave direction in this session (Fig.4). Whereas, in the pre-monsoon, the circulation of the sediments found to be at lower part of the study area due to the dominate wave and current action along the shore (Fig.5). Basically, a sediment particle will be suspended when the vertical velocity of the fluid motion becomes greater than the settling velocity of the particle. So, in the case of wave field, the vertical motion must result from the combined effects of turbulence and wave orbital motion. Here another phenomenon also acts on the sediments, i.e. gravity of the sediments suspended in the ocean, as the heavy sediments get deposited near shore, whereas the lighter sediments float. The wave direction in the post-monsoon and pre-monsoon is shown in Fig.4 and Fig.5. It is found that SSC decreased rapidly with the increase in distance (0-10kilometers) from the shoreline as well as bathymetry level of 5-10 meters. Also, the effect of the wave shoaling in the deeper water is significantly less, which caused sparely distribution sediment concentration. The SSC, beyond 5000 meters from the shoreline and below 10-20 meters depth, are rarely observed as they cannot be measured

at that depth, which is one of the limitations of the optical data. The movement of SSC indicates that the SSC have a positive correlation with wave direction and littoral current. We assigned weight to the layer based on the deposition along the shore. Most of the southern part of the study area was found to the high concentration of suspended matter during pre and post monsoon seasons, which was derived from the single band model with very less RMS error, i.e. 0.19 unit. The middle part was found to have cyclic concentration as it experienced seasonal erosion of the shore and deposition sediments near the beach. The north most part of the study area was found have less concentration of the suspended sediments during pre and post monsoon seasons.

<Insert Figure 4 Suspended sediments in the pre monsoon >

<Insert Figure 5 Suspended sediments in the post-monsoon >

5 Discussion and Conclusion

The paper explored the concentration and movement of suspended particles along the Thiruvananthapuram coast. The findings revealed that p the sediment concentration decreased rapidly with the increase in distance to the beach and depth to the seabed. As the bathymetry increased, low amount of sediments available moved towards the shore to cause low concentrations in the surface water. Wave, frequent phenomena, at comparatively large distance in deeper water, caused sparely distribution of sediments. Thus, the sediments were concentrated at a lower depth in high bathymetry (≥10m) and distance more than 2 km from the shoreline. The study found higher suspended sediments concentration near the coast particularly at surf zone and having less bathymetry up to 50-100 m, and it disappears with increase in bathymetry because the phenomenon of wave breaking and littoral current do not let the suspended sediments move far beyond the coast.

The study provides interesting visions for monitoring the suspended sediments at near shore after radiometric and geometric corrections. Another prospect of this study is the analysis of factors affecting the particles to be suspended in the near shore as well as offshore. OLI (30m) is having spectral range 0.45 to 0.88 nm for visible as well as NIR, demonstrated the best

details for spectral response analysis. This analysis revealed that the high reflection in near IR expressed the high concentration of SSC and, in contrast, the high reflection in the visible range showed lower concentration of suspended sediments. Suspended sediments moved north-south during post monsoon and reversed their direction during post monsoon season under the influence of monsoon winds. Mapping the spatial distribution of suspended materials using remotely sensed data would help in the management of coastal environment. Further study in this direction can aid the determination of the point and non- point source of water bodies, which discharge in the ocean. Hence, remote sensing data can potentially be utilized as a tool for monitoring the sediments in the ocean.

Acknowledgement:

The authors declare that there is no conflict of interests regarding the publication of this paper. KS and BRT were formulated the research work and processed data; KS, PK, and BRT were implemented technique and KS, PK and BSC, PKJ were discussed, validated and designed the article.

References

1. Byers, Alton C.: Soil loss and sediment transport during the storms and landslides of May 1988 in Ruhengeri prefecture, Rwanda, Natural Hazards, 5(3),279-292, 1992.
2. Curran, P.J., and Novo, E.M.M.: The relationship between suspended sediment concentration and remotely sensed spectral radiance: a review, Journal of Coastal Research, 4(3),351–368, 1988.
3. European Centre for Medium-Range Weather Forecasts, ERA Interim (www.ecmwf.int)
4. Gao, P.: Understanding watershed suspended sediment transport. Progress in Physical Geography, 32 (3), 243–263, 2008.
5. Gerald k. Moore: Satellite remote sensing of water turbidity / Sonde de télémesure par satellite de la turbidité de l'eau, Hydrological Sciences Bulletin, 25(4), 407-421, 1980.
6. Gordon, H., Wang, M.: Retrieval of water-leaving radiance and aerosol optical thickness over the oceans with SeaWiFS: a preliminary algorithm, Appl. Opt., 33, 443-452, 1994.
7. Islam, M.R., Yamaguchi, Y., and Ogawa, K.: Suspended sediment in the Ganges and Brahmaputra River in Bangladesh: observation from TM and AVHRR data, Hydrological Processes, 15(3), 493–509, 2001.
8. Kaliraj, S., Chandrasekar, N., Magesh, N.S.: Evaluation of coastal erosion and accretion processes along the southwest coast of Kanyakumari, Tamil Nadu using geospatial techniques, Arab J Geosci., doi: 10.1007/s12517-013- 1216-7, 2013b.

9. Kaliraj, S., Chandrasekar, N., Magesh, N.S.: Impacts of wave energy and littoral currents on shoreline erosion/ accretion along the south-west coast of Kanyakumari, Tamil Nadu using DSAS and geospatial technology, Environ Earth Sci.,doi: 10.1007/s12665-013-2845-6, 2013a.
10. Kaliraj, S., Chandrasekar, N.: Spectral recognition techniques and MLC of IRS P6 LISS III image for coastal landforms extraction along South West Coast of Tamilnadu, India, Bonfring, Int J Adv Image Process, 2(3), 01–07, 2012.
11. Katlane, R., Nechad, B., Ruddick, K., Zargouni, F.: Optical remote sensing of turbidity and total suspended matter in the Gulf of Gabes, Arab J Geosci, 6, 1527–1535, 2013.
12. Kisi, O.:. Modeling discharge-suspended sediment relationship using least square support vector machine. Journal of Hydrology, 456-457, 110–120, 2012
13. Kronvang, B., Laubel, A., Grant, R.: Suspended Sediment and Particulate Phosphorus Transport and Delivery Pathways in an Arable Catchment, Gelbaek Stream, Denmark, Hydrological Processes, 11(6), 627-642, 1997.
14. Marcus, W.A., and Fonstad, M.A.: Remote sensing of rivers: the emergence of a subdiscipline in the river sciences, Earth Surface Processes and Landforms, 35(15), 1867–1872, 2010.
15. Meteorological Center, IMD, Thiruvananthapuram (https://www.imdtvm.gov.in)
16. Nechad, B., Ruddick, K., Park, Y.: Calibration and validation of a generic multi-sensor algorithm for mapping of total suspended matter in turbid waters, Remote Sensing of Environment, 114, 854–866, 2010.
17. Neukermans, G., Ruddick, K., Bernard, E., Ramon, D., Nechad, B., Deschamps, P.Y.: Mapping total suspended matter from geostationary satellites: a feasibility study with SEVIRI in the Southern North Sea, Opt. Express 17, 14029–14052, 2009.
18. Ontowirjo, Budianto, Paris, Rapha, Mano, Akira: Modeling of coastal erosion and sediment deposition during the 2004 Indian Ocean tsunami in Lhok Nga, Sumatra, Indonesia, Natural Hazards, 65(3), 1967-1979, 2013.
19. Panwar, S., Agarwal, V., Chakrapani, G. J.: Morphometric and sediment source characterization of the Alaknanda river basin, headwaters of river Ganga, India, Natural Hazards, 1-23, 2017.
20. Qu, L.: Remote sensing suspended sediment concentration in the Yellow River, Ph.D. dissertation paper 383, University of Connecticut, website accessed December 2014 at http://digitalcommons.uconn.edu/dissertations/383/, 2014.
21. Rawat, Pradeep K., Tiwari, P. C., Pant, C. C., Sharama, A. K., Pant, P. D.: Modelling of stream run-off and sediment output for erosion hazard assessment in Lesser Himalaya: need for sustainable land use plan using remote sensing and GIS: a case study, Natural Hazards, 59 (3), 1277-1297, 2011.
22. Sinha, P. C., Guliani, Pragya, Jena, G. K., Rao, A. D., Dube, S. K., Chatterjee, A. K., Murty, Tad : A Breadth Averaged Numerical Model for Suspended Sediment Transport in Hooghly Estuary, East Coast of India, Natural Hazards, 32(2), 239-255, 2004.
23. Tassan, S.: A procedure to determine the particulate content of shallow water from Thematic Mapper data, Int J Rem Sens., 19, 557–562, 1998.

24. Vanhellemont, Q., Neukermans, G., Ruddick, K.: Synergy between polar-orbiting and geostationary sensors: Remote sensing of the ocean at high spatial and high temporal resolution, Remote Sens. Environment, 146, 49–62, 2014.
25. Wang, J.J., and Lu, X.X.: Estimation of suspended sediment concentrations using Terra MODIS: an example from the Lower Yangtze River, China, Science of the Total Environment 408, (5), 1131–1138, 2010.
26. Wang, J.J., Lu, X.X., Liew, S.C., Zhou, Y.: Retrieval of suspended sediment concentrations in large turbid rivers using Landsat ETM plus : an example from the Yangtze River, China, Earth Surface Processes and Landforms, 34, 1082-1092, 2009.
27. Warrick, J.A., Merters, L.A.K., Siegel, D.A., Mackenzie, C.: Estimating suspended sediment concentrations in turbid coastal waters of the Santa Barbara Channel with SeaWiFS, Int J Rem Sens., 25, 1995–2002, 2004.
28. Whitelock, C.H., Witte, W.G., Taly, T.A., Morris, W.D., Usry, J.W., Poole, L.R.: Research for reliable quantification of water sediment concentrations from multispectral scanner remote sensing data. US National Aeronautics and Space Administration, Langley Research Center, Hampton, VA, NASA-TM-82372, 243-255, 1981.
29. Yanjiao, W., Feng, Y., Peiqun, Z., Wenjie, D.: Experimental research on quantitative inversion models of suspended sediment concentration using remote sensing technology, Chinese GeographSci.,17 (3), 243–249, 2007.
30. Zhang, Y., Pulliainen, J., Koponen, S., Hallikainen, M.: Water quality retrievals from combined Landsat TM data and ERS-2 SAR data in the Gulf of Finland, IEEE Trans Geosci Remote Sens., 41, 622-629, 2003.

List of Figures

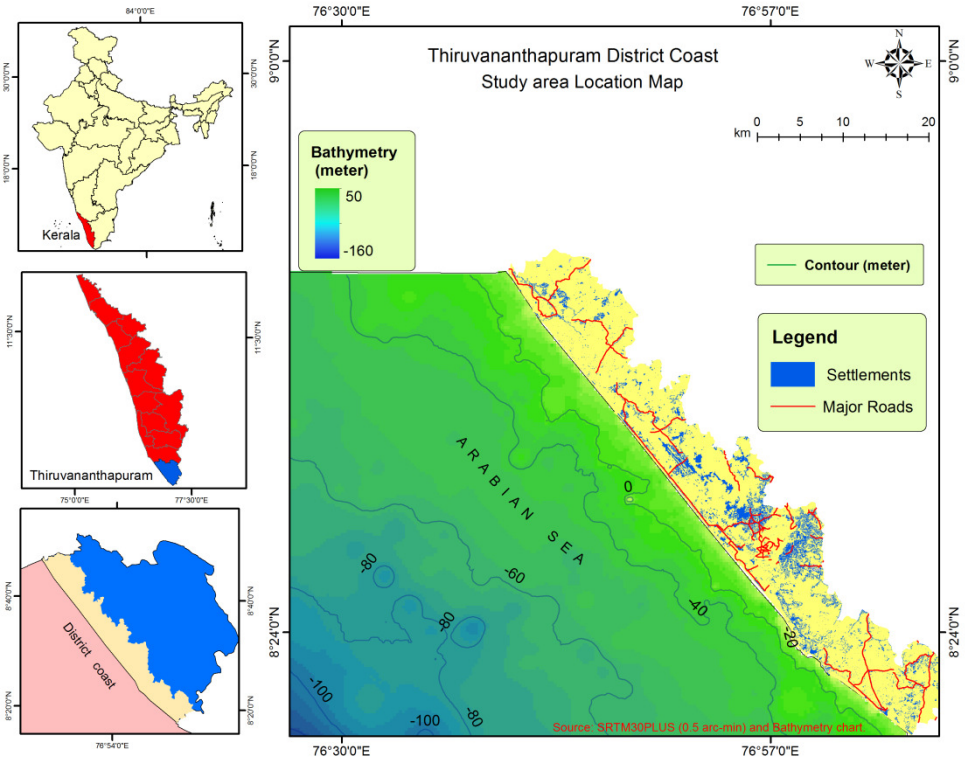

Figure1: Location map of study area.

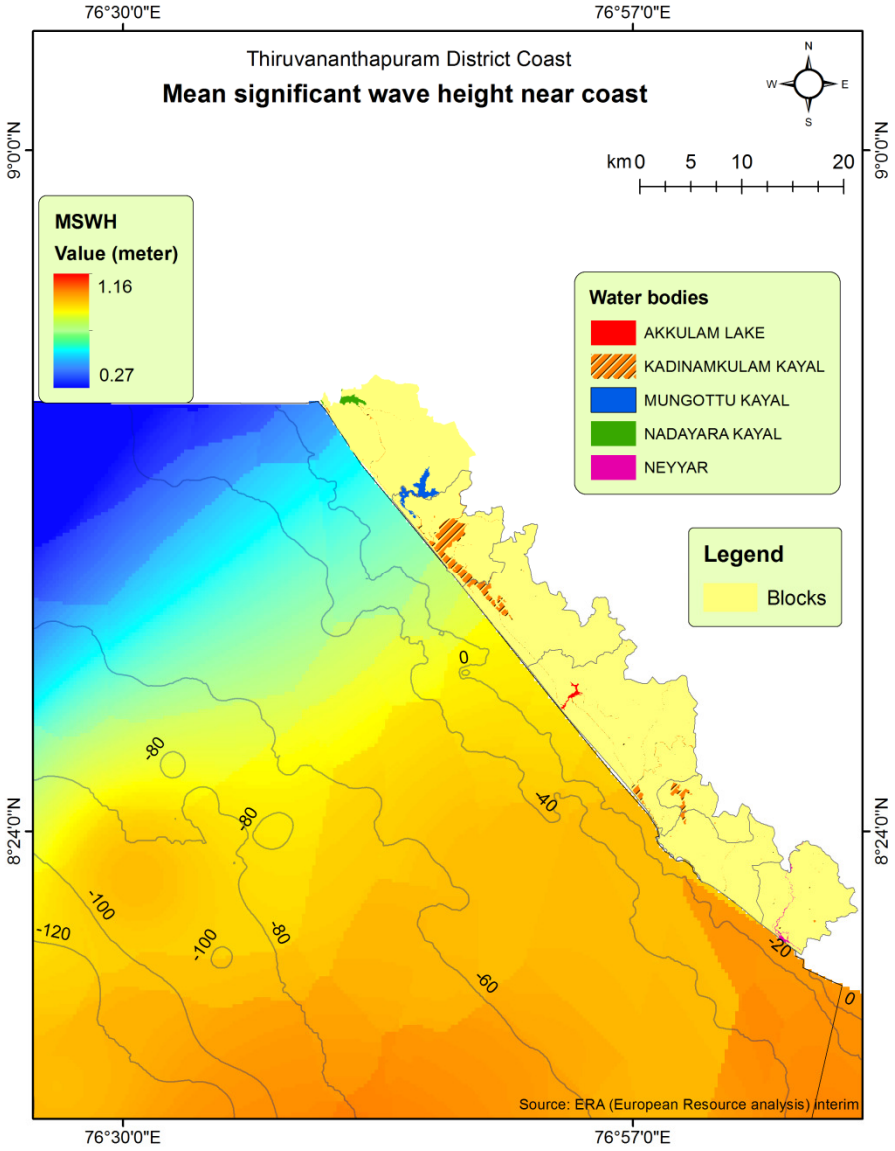

Figure 2: Mean significant wave height along the coast.

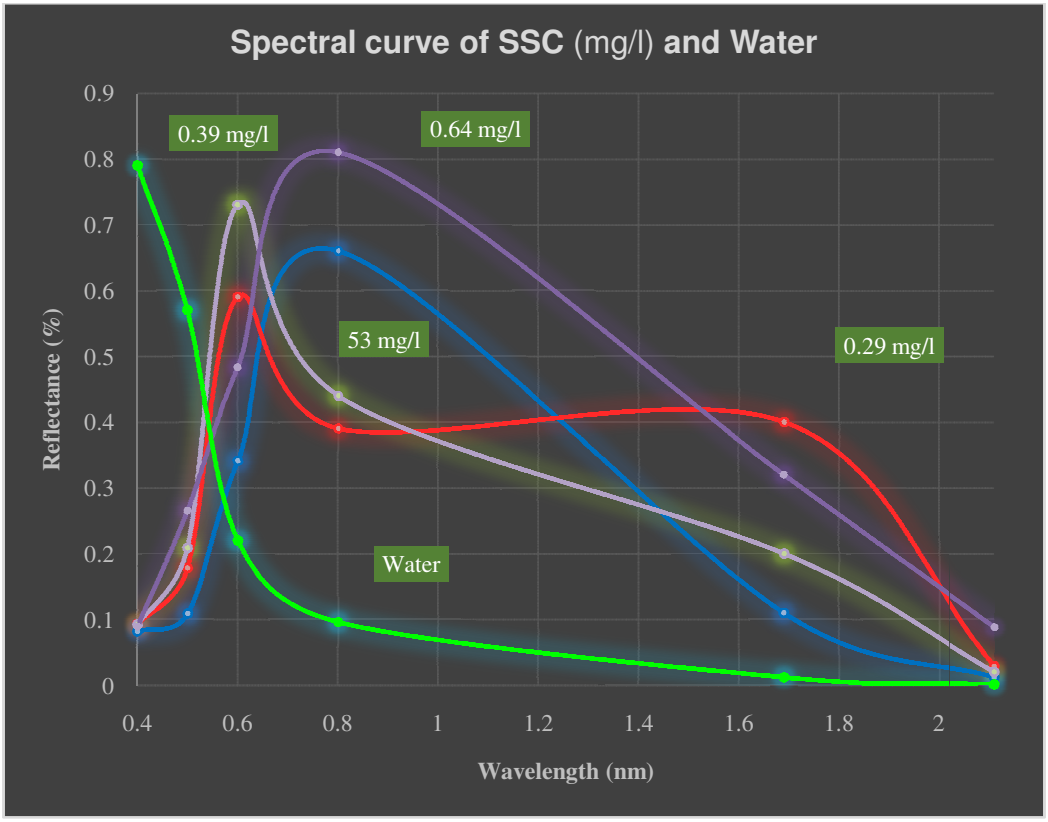

Figure 3: Spectral reflectance curve.

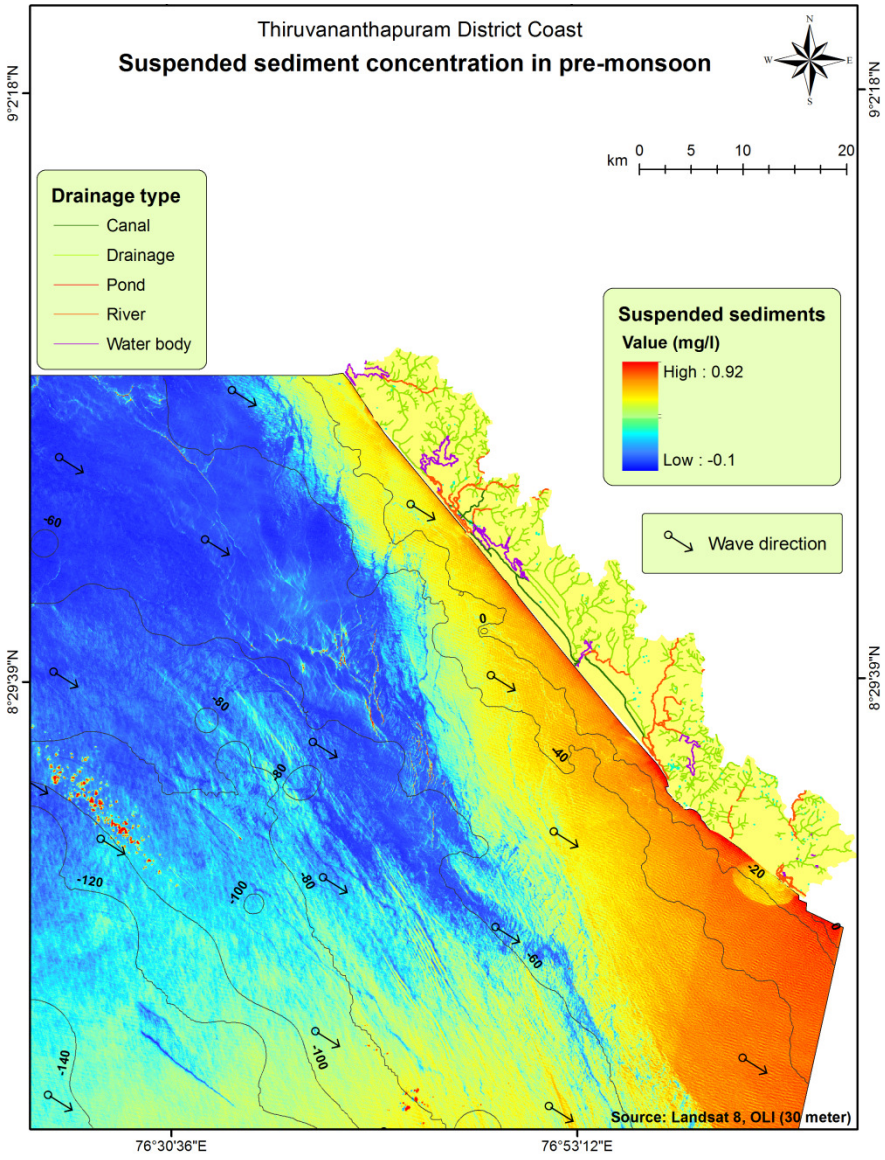

409

410

411 **Figure 4: Suspended sediments in the pre monsoon.**

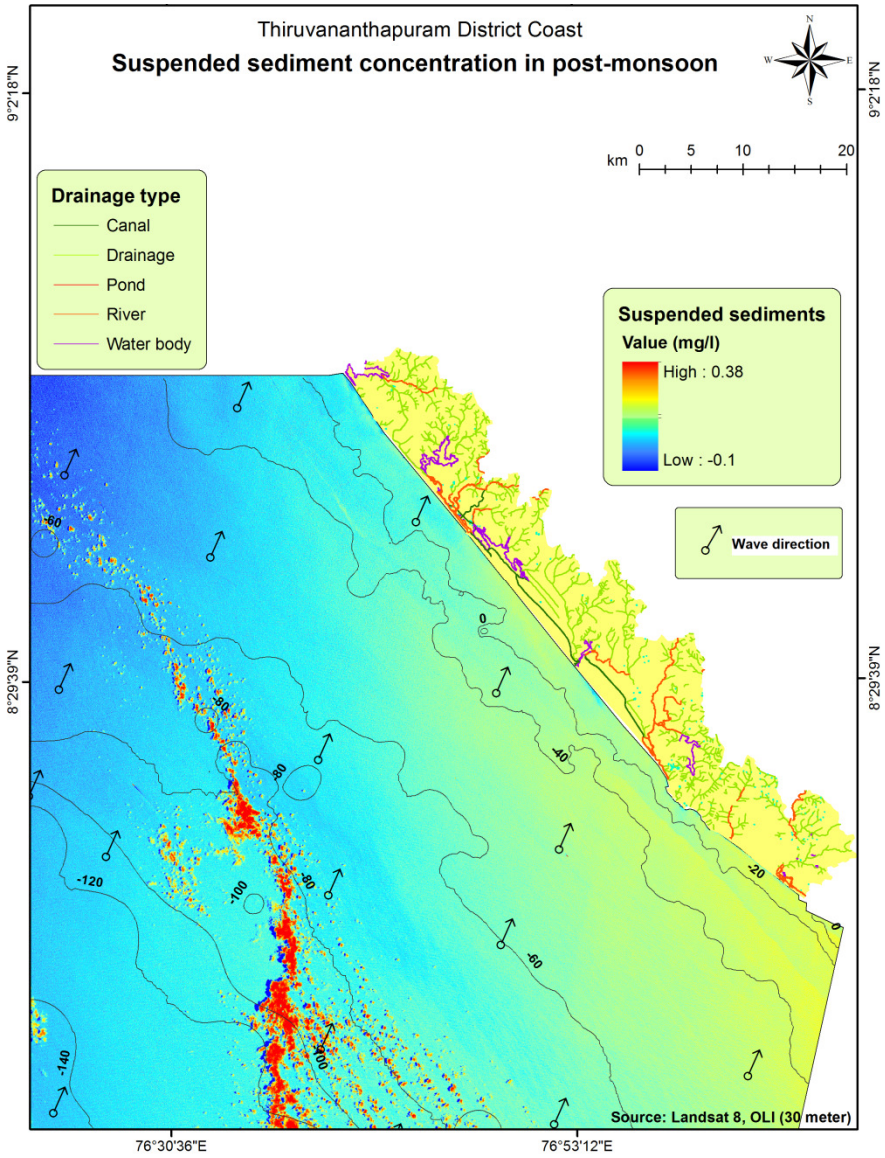

Figure 5: Suspended sediments in the post-monsoon.